ACS APPLIED MATERIALS & INTERFACES

Research Article

Cite This: ACS Appl. Mater. Interfaces 2019, 11, 29072−29077

www.acsami.org

Ruthenium Ion-Complexed Carbon Nitride Nanosheets with Peroxidase-like Activity as a Ratiometric Fluorescence Probe for the Detection of Hydrogen Peroxide and Glucose

Wenfang Deng,[†,‡,§] Yi Peng,[‡,§] Hui Yang,[†] Yueming Tan,*[,†,‡] Ming Ma,[†] Qingji Xie,[†] and Shaowei Chen*[,‡]

[†]Key Laboratory of Chemical Biology and Traditional Chinese Medicine Research (Ministry of Education), College of Chemistry and Chemical Engineering, Hunan Normal University, Changsha, Hunan 410081, China

[‡]Department of Chemistry and Biochemistry, University of California, 1156 High Street, Santa Cruz, California 95064, United States

Supporting Information

ABSTRACT: Detection of hydrogen peroxide is of great significance for clinical diagnosis and biomedical research. Ratiometric detection represents an effective method that is generally based on horseradish peroxidase. In the present study, ruthenium ion-complexed carbon nitride (Ru−C_3N_4) nanosheets are found to serve as a peroxidase mimic and can catalyze the conversion of *o*-phenylenediamine to fluorescent 2,3-diaminophenazine in the presence of H_2O_2. The produced 2,3-diaminophenazine also results in the apparent quenching of the Ru−C_3N_4 photoluminescence due to the inner filter effect. These unique characteristics can be exploited for the construction of an effective, peroxidase-free ratiometric fluorescence framework for the detection of H_2O_2 and glucose, which has also been used in the successful detection of glucose in human serum. Results from this study not only demonstrate a new peroxidase mimic but also provide a novel ratiometric fluorescence platform for the detection of H_2O_2 and metabolites involving reactions of H_2O_2 generation in the absence of horseradish peroxidase.

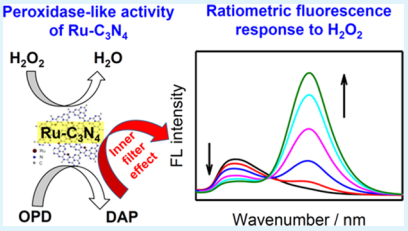

KEYWORDS: *ion complexation, carbon nitride, peroxidase mimic, ratiometric fluorescence probe, hydrogen peroxide, glucose*

INTRODUCTION

Hydrogen peroxide (H_2O_2) is a critical metabolite in cells and plays a vital role in physiological health. For instance, H_2O_2 is a signal molecule related to oxidative stress and physiological activity.[1] An abnormal level of H_2O_2 can increase the risk of central nervous system diseases and cancers.[2] Therefore, the detection of H_2O_2 is of great significance for biomedical research and clinical diagnosis. Thus far, a range of techniques have been reported for H_2O_2 detection, including electrochemistry,[3] colorimetry,[4] fluorescence,[5] and chemiluminescence.[6] Of these, the fluorescence method shows many advantages, such as rapid analysis, good sensitivity, and high selectivity. Compared with single fluorescence measurement, ratiometric fluorescence measurements can minimize erroneous signals from environmental influences and exhibit improved sensitivity and precision, because it is based on the concurrent recording of two fluorescence signals at a single excitation wavelength.[7] For instance, ratiometric fluorescence detection of H_2O_2 has been reported by using horseradish peroxidase (HRP) as the enzymatic catalyst.[8,9] In one study,[8] HRP catalyzes the oxidation of nonfluorescent *o*-phenylenediamine (OPD) to fluorescent 2,3-diaminophenazine (DAP), and DAP quenches the fluorescence of graphitic carbon nitride (C_3N_4). These observations can be exploited for the construction of a ratiometric fluorescence platform for the detection of H_2O_2 based on the decrease of the C_3N_4 fluorescence and the enhancement of the DAP fluorescence. However, reports of ratiometric fluorescence detection of H_2O_2 in the absence of HRP have been scarce. Notably, the use of peroxidase mimetics as the fluorescence probe may enable the detection of H_2O_2 in the absence of HRP, which will be useful for living cell analysis in the future.

Enzyme mimetics hold great potential in replacing natural enzymes because of their low costs and high stability.[10,11] In 2007, magnetic Fe_3O_4 nanoparticles were found to behave as peroxidase mimics.[12] Ever since, a vast variety of (nano)-materials also exhibit peroxidase-like activities. These include noble metals,[13,14] metal oxides,[15−17] metal complexes,[18−20] and carbon materials.[21,22] C_3N_4 and metal nanoparticles/C_3N_4 composite materials have also been exploited as peroxidase mimetics for the colorimetric detection of H_2O_2.[23−25] However, ratiometric fluorescence detection of H_2O_2 has not been achieved based on peroxidase mimetics, which is anticipated to exhibit higher sensitivity and better selectivity than conventional colorimetric detection. This is the main motivation of the present work.

In an earlier study,[26] we demonstrated that the abundant pyridinic nitrogen of carbon nitride nanosheets could be

Received: June 18, 2019
Accepted: July 17, 2019
Published: July 17, 2019

DOI: 10.1021/acsami.9b10715
ACS Appl. Mater. Interfaces 2019, 11, 29072−29077

exploited for the complexation of ruthenium(II) ions (Ru−C_3N_4), which exhibited high electrocatalytic activity toward hydrogen evolution reaction. In the present study, it was found that Ru−C_3N_4 also shows high peroxidase-like activity and might be exploited for the construction of a novel, effective ratiometric fluorescence platform for the detection of H_2O_2 (Scheme 1). Experimentally, OPD was oxidized by H_2O_2 to

Scheme 1. Schematic Illustration of Ru−C_3N_4 as a Peroxidase Mimic

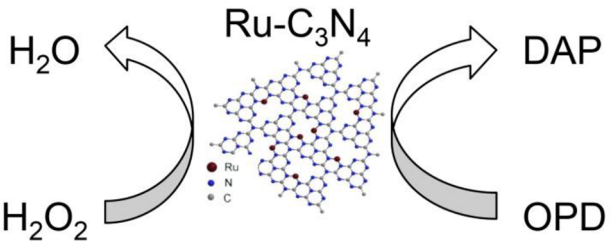

produce DAP in the presence of Ru−C_3N_4 (in place of HRP) that exhibited a fluorescence emission at 565 nm, and concurrently the fluorescence emission of Ru−C_3N_4 (at 455 nm) was quenched by the generated DAP due to the inner filter effect. The diminishment of the Ru−C_3N_4 fluorescence together with the enhancement of the DAP fluorescence enables the ratiometric fluorescence detection of H_2O_2. To the best of our knowledge, this is the first demonstration of peroxidase-like activity by Ru−C_3N_4 nanocomposites and its use as a peroxidase-free ratiometric fluorescence probe for the detection of H_2O_2. The detection limit for H_2O_2 (50 nM) is amongst the lowest ones reported previously, highlighting an effective strategy for the sensitive detection of H_2O_2. The unique property is also exploited for the sensitive and selective detection of glucose, which is known to generate H_2O_2 when catalyzed by glucose oxidase (GOx).

EXPERIMENTAL SECTION

Chemicals. Glucose oxidase (GOx, 150 kU g^{-1}) was obtained from Sigma-Aldrich. Melamine, *o*-phenylenediamine (OPD), and hydrogen peroxide (H_2O_2, 30 wt.%) were purchased from Sinopharm Chemical Reagents Co. Ltd. Ruthenium(III) chloride ($RuCl_3$), glucose, maltose, sucrose, galactose, bovine serum albumin (BSA), ascorbic acid, uric acid, and amino acids were purchased from Aladdin Chemicals Co., Ltd. Human serum samples were obtained from healthy volunteers in the Fourth Hospital of Changsha. All other reagents were of analytical or better grade and used as received. Acetate buffer solution was prepared with 0.10 M acetic acid and sodium acetate (pH 4.5). Phosphate buffer solution (PBS, pH 7.0) was prepared with 0.10 M KH_2PO_4 and Na_2HPO_4. Water was purified with a Millipore Milli-Q System (resistivity 18.3 MΩ·cm).

Preparation of Ru−C_3N_4. The preparation of Ru−C_3N_4 has been detailed previously.[26] Experimentally, graphitic C_3N_4 nanosheets were first produced by the thermal treatment of melamine in air followed by sonication in water:[27,28] (i) melamine (10 g) was loaded into a ceramic crucible with a cover, which was put into in a muffle furnace and heated at 600 °C for 3 h at the heating rate of 2.3 °C min^{-1}, and (ii) 50 mg of the above products were dispersed into 50 mL of H_2O, and C_3N_4 thin layers were formed by sonication overnight.

Ru−C_3N_4 was then prepared by thermal refluxing of the obtained C_3N_4 and $RuCl_3$ in water.[26] In brief, 56 mg of $RuCl_3$ was added to the above C_3N_4 dispersion, and the mixture was refluxed for 4 h. Centrifugation was then used to separate the product, and excess ruthenium ions were removed by washing the collected solids with water and ethanol.

Characterization. High-resolution transmission electron microscopy (TEM) images were acquired with a TECNAI F-30 transmission electron microscope. X-ray photoelectron spectroscopy (XPS) studies were carried out with a Thermo Fisher XPS instrument. Ultraviolet−visible (UV−vis) absorption spectra were collected with a Shimadzu UV2450 spectrophotometer. Fluorescence spectroscopic studies were performed on a Hitachi F-7000 spectrophotometer. An Agilent 1260-7700e instrument was used for inductively coupled plasma mass spectrometric (ICP-MS) analysis. Zeta potentials were evaluated with a Malvern Zetasizer Nano Z Analyzer.

Detection of H_2O_2. 10 μL of a H_2O_2 aqueous solution at different concentrations was added into 1 mL of the 0.10 M acetate buffer solution (pH 4.5) containing 50 μg mL^{-1} Ru−C_3N_4 and 0.2 mM OPD. After incubation at 25 °C for 10 min, fluorescence measurements were carried out with the excitation set at 370 nm.

Detection of Glucose. Experimentally, a 10 μL solution containing 0.10 M PBS (pH 7.0), 0.50 mg mL^{-1} GOx and glucose of different concentrations was first prepared. After incubation at 25 °C for 30 min, the solution was transferred into a 1 mL 0.10 M acetate buffer solution (pH 4.5), which contained 50 μg mL^{-1} Ru−C_3N_4 and 0.2 mM OPD. Additional incubation was allowed for 10 min at 25 °C, before fluorescence spectra were acquired at 370 nm excitation. To detect glucose in human serum, the sample was diluted with PBS by a factor of 20, before fluorescence spectra were collected.

RESULTS AND DISCUSSION

Ru−C_3N_4 was prepared by the thermal refluxing of graphitic C_3N_4 and $RuCl_3$ in aqueous solution, where the ruthenium metal centers were incorporated within the C_3N_4 scaffold by coordination to two pyridinic nitrogen moieties (RuN_2), as described previously (Scheme 1).[26] The morphology of Ru−C_3N_4 was first characterized by TEM measurements. As shown in Figure 1a,b, Ru−C_3N_4 shows a nanosheet structure of a few tens of nanometers across, similar to that of pristine C_3N_4 (Figure S1a). Figure 1c shows the high-angle annular dark-field scanning TEM (HAADF-STEM) image of Ru−C_3N_4 and elemental maps based on energy-dispersive X-ray (EDX) analysis, where the C, N, Ru, and Cl elements can be seen to be uniformly distributed in the sample. Note that no crystalline Ru species was found in Ru−C_3N_4, as demonstrated in high-resolution TEM and X-ray diffraction studies.[26] ICP-MS measurements showed that the Ru content in Ru−C_3N_4 was ca. 9.97 atom %.

The chemical composition of Ru−C_3N_4 was further examined by XPS measurements. From the survey spectrum in Figure 1d, one can readily identify the C, N, Ru, and Cl elements. Figure 1e shows the corresponding high-resolution spectrum of the Ru 3d and C 1s electrons. The Ru $3d_{5/2}$ and $3d_{3/2}$ electrons can be deconvoluted at 281.3 and 285.2 eV, which are consistent with those of Ru(II) in ruthenium bipyridine complexes,[29] suggesting that the Ru centers were mainly in the +2 valence state, as detailed previously.[26] Two C 1s subpeaks can be found at 284.5 and 288.0 eV, which can be assigned to the defective C in sp^3 C−C and sp^2-hybridized C in N—C═N, respectively. Notably, the latter binding energy (288.0 eV for C in N—C═N) shows a marked blue shift for Ru−C_3N_4, as compared to that (287.3 eV) of pristine C_3N_4 (Figure S1b), due to the formation of Ru−N coordination bonds.[26] Two nitrogen species can be identified from the deconvolution of the N 1s peak for Ru−C_3N_4, the sp^3-hybridized tertiary N (N−$(C)_3$) at 399.7 eV, and the sp^2-hybridized pyridinic N (C—N═C) at 398.4 eV (Figure 1f). Again, because of ruthenium ion complexation, the binding energy of N in N—C═N for Ru−C_3N_4 is higher than that for pristine C_3N_4 (397.8 eV, Figure S1c). The Cl 2p peak for Ru−

DOI: 10.1021/acsami.9b10715
ACS Appl. Mater. Interfaces 2019, 11, 29072−29077

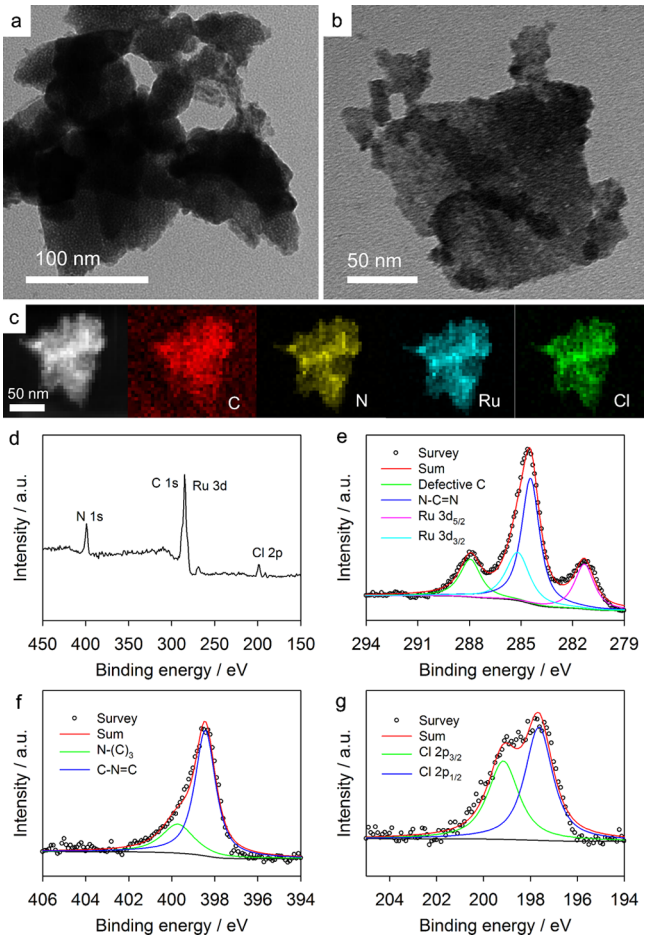

Figure 1. (a, b) Representative TEM images, (c) HAADF-STEM image and elemental maps, and (d) XPS survey spectrum of Ru−C_3N_4. High-resolution XPS scans of the (e) Ru 3d and C 1s, (f) N 1s, and (g) Cl 2p electrons in Ru−C_3N_4.

C_3N_4 in Figure 1g is fitted with Cl $2p_{3/2}$ at 199.2 eV and Cl $2p_{1/2}$ at 197.6 eV, indicating the presence of chloride ions in the outer sphere to neutralize the charge. These results are consistent with those obtained previously.[26] In addition, the atomic ratio of C/N in both C_3N_4 and Ru−C_3N_4 is found to be close to 3:4 by elemental analysis (Table S1).

The catalytic activity of Ru−C_3N_4 toward the oxidation of peroxidase substrate OPD in the presence of H_2O_2 was then tested in the acetate buffer (pH 4.5) at 25 °C. After incubation of the solution containing 0.2 mM OPD, 1 mM H_2O_2, and 50 μg mL^{-1} Ru−C_3N_4 for 10 min, the solution was found to exhibit a yellow color (Figure 2a) with a sharp absorption peak at 450 nm (Figure 2b), indicating effective catalysis of the oxidation of OPD to yellow DAP by Ru−C_3N_4 in the presence of H_2O_2 (Scheme 1). By contrast, in the absence of Ru−C_3N_4 or H_2O_2, the solution remained colorless (Figure 2a), and exhibited no apparent absorption peak at 450 nm (Figure 2b), suggesting that the direct oxidation of OPD by Ru−C_3N_4 or H_2O_2 alone was kinetically sluggish. Note that whereas C_3N_4 has been reported to show peroxidase-like activity,[23] we found that this catalytic activity was markedly lower than that of Ru−C_3N_4 under the same reaction conditions. As the peroxidase-like activity of Ru−C_3N_4 reached the maximum at pH 4.5 (Figure S2), all the catalytic experiments were conducted in the 0.10 mM acetate buffer (pH 4.5).

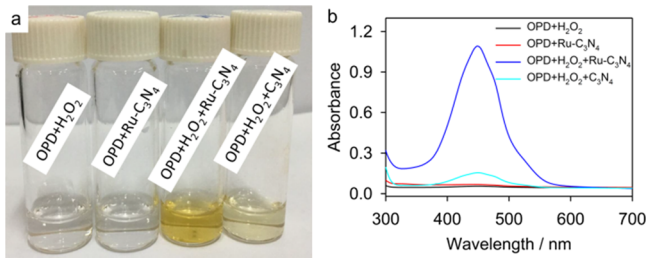

Figure 2. (a) Photograph and (b) UV−vis absorption spectra of OPD + H_2O_2, OPD + Ru−C_3N_4, OPD + H_2O_2 + Ru−C_3N_4, and OPD + H_2O_2 + C_3N_4. Experiments are carried out in 0.1 mM acetate buffer (pH 4.5) containing 0.2 mM OPD, 1 mM H_2O_2, 50 μg mL^{-1} Ru−C_3N_4, and 50 μg mL^{-1} C_3N_4.

The steady-state kinetic parameters for OPD and H_2O_2 in the catalytic reaction were then quantitatively evaluated. From the Michaelis−Menten and Lineweaver−Burk plots in Figure S3, the Michaelis constant (K_m) and maximal reaction velocity (V_{max}) for Ru−C_3N_4 toward OPD were estimated to be 0.068 mM and 8.33 μM s^{-1}, respectively. The small K_m value indicates that Ru−C_3N_4 possessed a high binding affinity toward H_2O_2, while the large V_{max} value indicates that Ru−C_3N_4 exhibited a high catalytic activity. Similarly, for Ru−C_3N_4 toward H_2O_2 (Figure S4), K_m is estimated to be 2.4 mM and V_{max} 41.66 μM s^{-1}. The K_m value toward H_2O_2 for Ru−C_3N_4 is much smaller than those for Ru frames (318 mM),[30] Pd nanoplates (4.4 mM),[31] and Fe_3O_4 nanoparticles (154 mM),[12] suggesting that the Ru−C_3N_4 has higher binding affinity toward H_2O_2 than the other peroxidase mimetics reported previously. Furthermore, the V_{max} value toward H_2O_2 for Ru−C_3N_4 is much larger than those for peroxidase mimetics reported previously (4.45 μM s^{-1} for Ru frames,[30] 3.906 μM s^{-1} for Pd nanoplates,[31] and 5.868 μM s^{-1} for Fe_3O_4 nanoparticles),[12] signifying the high peroxidase-like activity of Ru−C_3N_4. In addition to the high catalytic activity, Ru−C_3N_4 also showed excellent stability. After storage at ambient temperature for half a year, the catalytic activity of Ru−C_3N_4 was found to remain virtually unchanged.

The fluorescence property of Ru−C_3N_4 was further examined. From Figure S5a, Ru−C_3N_4 can be seen to exhibit an excitation peak at 370 nm and an emission peak at 455 nm; and at 370 nm excitation, the 455 nm fluorescence emission increases proportionally to the concentration of Ru−C_3N_4 (Figure S5b). Yet, from Figure 3a, one can see that this emission is markedly quenched after incubation of 50 μg mL^{-1} Ru−C_3N_4 with 0.2 mM OPD and 1 mM H_2O_2 in 0.1 mM acetate buffer (pH 4.5) at 25 °C for 10 min. In addition, a new fluorescence peak emerges at 565 nm. This is due to the oxidation of OPD to fluorescent DAP catalyzed by Ru−C_3N_4 in the presence of H_2O_2. By contrast, OPD or H_2O_2 alone shows no influence on the fluorescence of Ru−C_3N_4.

To reveal the mechanism of the quenching of Ru−C_3N_4 fluorescence, the lifetime of Ru−C_3N_4 emission was measured and compared in the absence and presence of DAP. From Figure 3b, it can be seen that the fluorescence decay profiles of Ru−C_3N_4 remain virtually unchanged before and after the quenching by DAP, indicating no energy or electron transfer between Ru−C_3N_4 and DAP. Additionally, as the zeta potentials of Ru−C_3N_4, OPD, and DAP are all positive in 0.10 mM acetate buffer (pH 4.5) (Figure S6), it is unlikely that Förster resonance energy transfer occurred, because of electrostatic repulsion between Ru−C_3N_4 and DAP. From

DOI: 10.1021/acsami.9b10715
ACS Appl. Mater. Interfaces 2019, 11, 29072−29077

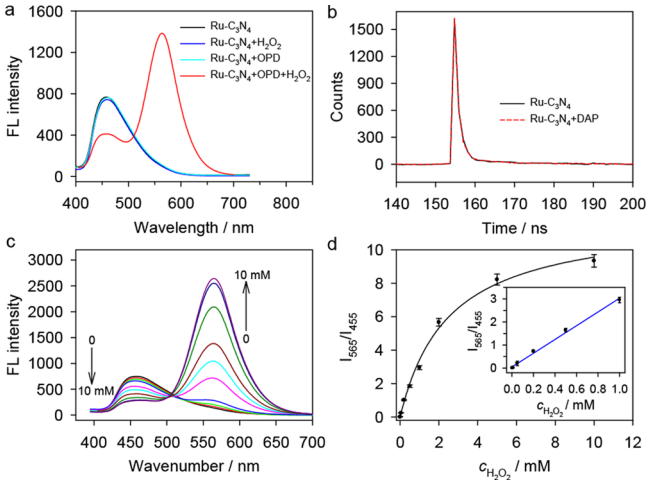

Figure 3. (a) Fluorescence emission spectra of Ru−C_3N_4, Ru−C_3N_4 + H_2O_2, Ru−C_3N_4 + OPD, and Ru−C_3N_4 + OPD + H_2O_2 at 370 nm excitation. Experiments are carried out in 0.1 mM acetate buffer (pH 4.5) for 10 min at 25 °C with 0.2 mM OPD, 1 mM H_2O_2, and 50 μg mL^{-1} Ru−C_3N_4. (b) Time-resolved fluorescence spectra of Ru−C_3N_4 in the absence and presence of DAP. (c) Fluorescence spectra of Ru−C_3N_4-based ratiometric fluorescence probe at 370 nm excitation in the presence of H_2O_2 at different concentrations. (d) Ratiometric fluorescence intensity (I_{565}/I_{455}) versus H_2O_2 concentration. Inset shows the linear range (calibration curve) for the detection of H_2O_2, where the symbols are experimental data and the line is linear regression.

Figure S7, one can see that there is a substantial overlap around 450 nm between the absorption spectrum of DAP and the fluorescence emission spectrum of Ru−C_3N_4 (at 370 nm excitation), so the quenching of Ru−C_3N_4 by DAP most likely arose from the inner filter effect.

Taken together, the experimental results presented above suggest that Ru−C_3N_4 exhibits apparent peroxidase-like activity and can catalyze the oxidation of OPD to fluorescent DAP in the presence of H_2O_2 as a peroxidase mimic. As the fluorescence of Ru−C_3N_4 is concurrently quenched by the generated DAP due to the inner filter effect, Ru−C_3N_4 can be exploited as an effective ratiometric fluorescence probe for the detection of H_2O_2. To achieve a high ratiometric response toward H_2O_2, several important parameters were optimized (Figure S8), that is, Ru−C_3N_4 concentration of 50 μg mL^{-1}, OPD concentration of 0.2 mM, solution pH of 4.5, and incubation time of 10 min.

Under these optimized experimental conditions, the Ru−C_3N_4-based ratiometric sensing platform was evaluated by fluorescence measurements, where emission spectra were recorded at the excitation wavelength of 370 nm in the presence of H_2O_2 at different concentrations. From Figure 3c, one can see that with the increase of the H_2O_2 concentration, the fluorescence emission intensity of Ru−C_3N_4 at 455 nm decreases accordingly, whereas the fluorescence emission of DAP at 565 nm becomes intensified. Figure 3d shows the variation of the ratiometric fluorescence intensity (I_{565}/I_{455}) with H_2O_2 concentration, where the linear range for H_2O_2 detection is estimated from 2×10^{-4} to 1.0 mM (inset to Figure 3d), with a linear regression equation of $y = 0.0502 + 2.97x$ ($R^2 = 0.9955$). The detection limit ($3\sigma/k$, with k being the slope of the curve and σ the standard deviation) is 50 nM, which is lower than the results in leading studies reported in recent literature (Table S2). Additionally, from Figure S9, other biologically relevant radicals (e.g., OH·, ClO·, O_2·, and ONOO·) can be seen to display no obvious influence on the ratiometric fluorescence detection of H_2O_2, indicating that the Ru−C_3N_4-based ratiometric sensing system has good specificity toward H_2O_2.

Since Ru−C_3N_4 shows apparent activity as a ratiometric fluorescence probe for H_2O_2 detection, it may be exploited further as a universal platform for the detection of metabolites that can generate H_2O_2 when catalyzed by enzymes in the human body. In this work, glucose was selected as the model target, as H_2O_2 can be readily produced from glucose using GOx as the catalyst. Experimentally, the optimal GOx concentration was ca. 0.5 mg mL^{-1}, with an incubation time of 30 min for glucose with GOx (Figure S10). From Figure 4a,

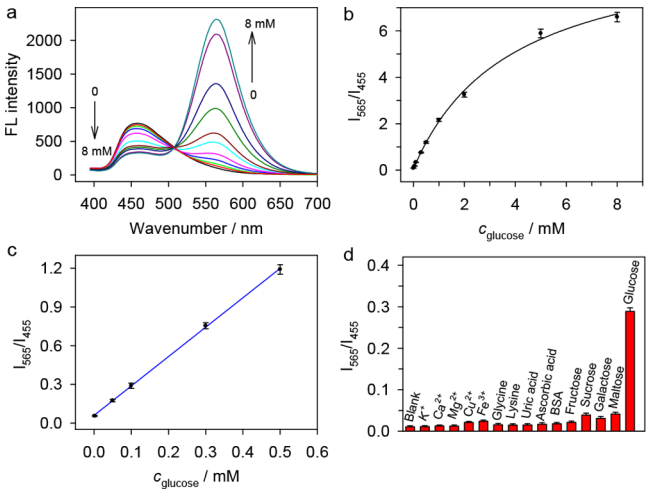

Figure 4. (a) Fluorescence emission spectra of Ru−C_3N_4-based ratiometric fluorescence probe at 370 nm excitation in the presence of glucose at different concentrations. (b) Ratiometric fluorescence intensity (I_{565}/I_{455}) versus glucose concentration. (c) Linear range (calibration curve) for the detection of glucose. (d) Selectivity of glucose detection. The concentration of glucose is 0.10 mM, of BSA is 1 mg mL^{-1}, and of all other interferents is 1 mM.

it can be seen that at increasing glucose concentrations, the intensity of the fluorescence emission of Ru−C_3N_4 at 455 nm decreases accordingly, while the fluorescence emission of DAP at 565 nm increases concurrently. Figure 4b shows the ratiometric fluorescence intensity (I_{565}/I_{455}) at different glucose concentrations, which features a linear range for glucose detection from 1×10^{-3} to 0.5 mM (Figure 4c), with a linear regression equation of $y = 0.0721 + 2.26x$ ($R^2 = 0.9936$). The detection limit is evaluated to be ca. 0.1 μM, which, again, is better than the leading literature results (Table S3).

The selectivity of the Ru−C_3N_4-based ratiometric sensing system was then investigated. From Figure 4d, no apparent influence was observed on the ratiometric fluorescence detection of glucose in the presence of a variety of potential interferents, such as maltose, galactose, sucrose, fructose, ascorbic acid, uric acid, lysine, glycine, and (transition) metal ions (e.g., Fe^{3+}, Cu^{2+}, Mg^{2+}, Ca^{2+}, and K^+), suggesting excellent selectivity and GOx-like catalytic specificity of Ru−C_3N_4. The Ru−C_3N_4-based ratiometric fluorescence probe was further tested for detecting glucose in human serum. As shown in Table S4, the performance of Ru−C_3N_4 was highly comparable to that of a commercial glucometer. The recovery efficiencies were between 95.5% and 104.3%, and the relative standard

DOI: 10.1021/acsami.9b10715
ACS Appl. Mater. Interfaces 2019, 11, 29072−29077

deviations were from 2.2% to 4.5%. These results suggest that the Ru−C_3N_4-based ratiometric sensing probe is capable of glucose detection in human serum.

CONCLUSIONS

In conclusion, Ru−C_3N_4 nanosheets were found to display apparent peroxidase-like activity and behave as a peroxidase mimic to catalyze the oxidation of OPD to fluorescent DAP in the presence of H_2O_2. As the fluorescence emission of Ru−C_3N_4 was concurrently quenched by the produced DAP by virtue of the inner filter effect, an effective ratiometric fluorescence platform was constructed for the detection of H_2O_2 and glucose. The detection limit was estimated to be 50 nM for H_2O_2 and 0.1 μM for glucose. Notably, the sensing platform was successfully used for detecting glucose in human serum, highlighting the significant potential in the sensitive detection of metabolites involving H_2O_2-generation reactions.

ASSOCIATED CONTENT

Supporting Information

The Supporting Information is available free of charge on the ACS Publications website at DOI: 10.1021/acsami.9b10715.

Additional experimental data: TEM and XPS characterization of C_3N_4, peroxidase-like activity of Ru−C_3N_4 at different solution pH, kinetic investigation of Ru−C_3N_4 toward OPD, kinetic investigation of Ru−C_3N_4 toward H_2O_2, fluorescence spectra of Ru−C_3N_4, zeta potentials of Ru−C_3N_4, OPD, and DAP, UV−vis absorption spectrum of DAP and fluorescence emission spectrum of Ru−C_3N_4, optimization of experimental parameters for H_2O_2 detection, selectivity of H_2O_2 detection, optimization of experimental parameters for glucose detection, elemental analysis results, performance comparison of H_2O_2 detection, performance comparison of glucose detection, and comparison of glucose detection in human serum with a commercial glucometer (PDF)

AUTHOR INFORMATION

Corresponding Authors

*E-mail: tanyueming0813@126.com; tanyueming0813@hunnu.edu.cn (Y.T).

*E-mail: shaowei@ucsc.edu (S.C.).

ORCID

Yi Peng: 0000-0002-5319-1336

Yueming Tan: 0000-0003-3356-9079

Shaowei Chen: 0000-0002-3668-8551

Author Contributions

§W.D. and Y.P. contributed equally to the work. The manuscript was written through contributions of all authors. All authors have given approval to the final version of the manuscript.

Notes

The authors declare no competing financial interest.

ACKNOWLEDGMENTS

Work at HNNU was supported by the National Natural Science Foundation of China (21705045 and 21775041), the Science and Technology Innovation Project of Hunan Province (2018RS3062), the Natural Science Foundation of Hunan Province (2018JJ2252), the Scientific Research Fund of Hunan Provincial Education Department (17A125), and the Science and Technology Project of Changsha (KQ1802036). Work at UCSC was supported by the National Science Foundation through grants CHE-1710408 and CBET-1848841. W.F.D. and Y.M.T. were supported by a fellowship from the China Scholarship Council.

REFERENCES

(1) Lin, M. T.; Beal, M. F. Mitochondrial Dysfunction and Oxidative Stress in Neurodegenerative Diseases. *Nature* **2006**, *443*, 787−795.

(2) Finkel, T.; Serrano, M.; Blasco, M. A. The Common Biology of Cancer and Ageing. *Nature* **2007**, *448*, 767−774.

(3) Li, Z.; Xin, Y.; Wu, W.; Fu, B.; Zhang, Z. Topotactic Conversion of Copper(I) Phosphide Nanowires for Sensitive Electrochemical Detection of H_2O_2 Release from Living Cells. *Anal. Chem.* **2016**, *88*, 7724−7729.

(4) Narayanaswamy, N.; Narra, S.; Nair, R. R.; Saini, D. K.; Kondaiah, P.; Govindaraju, T. Stimuli-Responsive Colorimetric and NIR Fluorescence Combination Probe for Selective Reporting of Cellular Hydrogen Peroxide. *Chem. Sci.* **2016**, *7*, 2832−2841.

(5) Abo, M.; Urano, Y.; Hanaoka, K.; Terai, T.; Komatsu, T.; Nagano, T. Development of a Highly Sensitive Fluorescence Probe for Hydrogen Peroxide. *J. Am. Chem. Soc.* **2011**, *133*, 10629−10637.

(6) Zhu, Q.; Huang, J.; Yan, M.; Ye, J.; Wang, D.; Lu, Q.; Yang, X. N-(Aminobutyl)-N-(ethylisoluminol)-Functionalized Gold Nanoparticles on Cobalt Disulfide Nanowire Hybrids for the Non-Enzymatic Chemiluminescence Detection of H_2O_2. *Nanoscale* **2018**, *10*, 14847−14851.

(7) Ajayaghosh, A.; Carol, P.; Sreejith, S. A Ratiometric Fluorescence Probe for Selective Visual Sensing of Zn^{2+}. *J. Am. Chem. Soc.* **2005**, *127*, 14962−14963.

(8) Liu, J.-W.; Luo, Y.; Wang, Y.-M.; Duan, L.-Y.; Jiang, J.-H.; Yu, R.-Q. Graphitic Carbon Nitride Nanosheets-Based Ratiometric Fluorescent Probe for Highly Sensitive Detection of H_2O_2 and Glucose. *ACS Appl. Mater. Interfaces* **2016**, *8*, 33439−33445.

(9) Ma, Y.; Cen, Y.; Sohail, M.; Xu, G.; Wei, F.; Shi, M.; Xu, X.; Song, Y.; Ma, Y.; Hu, Q. A Ratiometric Fluorescence Universal Platform Based on N, Cu Codoped Carbon Dots to Detect Metabolites Participating in H_2O_2-Generation Reactions. *ACS Appl. Mater. Interfaces* **2017**, *9*, 33011−33019.

(10) Lin, Y.; Ren, J.; Qu, X. Catalytically Active Nanomaterials: A Promising Candidate for Artificial Enzymes. *Acc. Chem. Res.* **2014**, *47*, 1097−1105.

(11) Wei, H.; Wang, E. Nanomaterials with Enzyme-Like Characteristics (Nanozymes): Next-Generation Artificial Enzymes. *Chem. Soc. Rev.* **2013**, *42*, 6060−6093.

(12) Gao, L.; Zhuang, J.; Nie, L.; Zhang, J.; Zhang, Y.; Gu, N.; Wang, T.; Feng, J.; Yang, D.; Perrett, S.; Yan, X. Intrinsic Peroxidase-Like Activity of Ferromagnetic Nanoparticles. *Nat. Nanotechnol.* **2007**, *2*, 577−583.

(13) Jv, Y.; Li, B. X.; Cao, R. Positively-Charged Gold Nanoparticles as Peroxidiase Mimic and Their Application in Hydrogen Peroxide and Glucose Detection. *Chem. Commun.* **2010**, *46*, 8017−8019.

(14) He, W.; Wu, X.; Liu, J.; Hu, X.; Zhang, K.; Hou, S.; Zhou, W.; Xie, S. Design of AgM Bimetallic Alloy Nanostructures (M = Au, Pd, Pt) with Tunable Morphology and Peroxidase-like Activity. *Chem. Mater.* **2010**, *22*, 2988−2994.

(15) André, R.; Natálio, F.; Humanes, M.; Leppin, J.; Heinze, K.; Wever, R.; Schröder, H. C.; Müller, W. E. G.; Tremel, W. V_2O_5 Nanowires with an Intrinsic Peroxidase-like Activity. *Adv. Funct. Mater.* **2011**, *21*, 501−509.

(16) Mu, J.; Wang, Y.; Zhao, M.; Zhang, L. Intrinsic peroxidase-like Activity and Catalase-like Activity of Co_3O_4 Nanoparticles. *Chem. Commun.* **2012**, *48*, 2540−2542.

(17) Liu, J.; Meng, L.; Fei, Z.; Dyson, P.; Jing, X.; Liu, X. MnO_2 Nanosheets as an Artificial Enzyme to Mimic Oxidase for Rapid and Sensitive Detection of Glutathione. *Biosens. Bioelectron.* **2017**, *90*, 69−74.

DOI: 10.1021/acsami.9b10715
ACS Appl. Mater. Interfaces 2019, 11, 29072−29077

(18) Wang, S.; Deng, W.; Yang, L.; Tan, Y.; Xie, Q.; Yao, S. Copper-Based Metal−Organic Framework Nanoparticles with Peroxidase-Like Activity for Sensitive Colorimetric Detection of *Staphylococcus aureus*. *ACS Appl. Mater. Interfaces* **2017**, *9*, 24440−24445.
(19) Zhang, J. W.; Zhang, H. T.; Du, Z. Y.; Wang, X.; Yu, S. H.; Jiang, H. L. Water-Stable Metal-Organic Frameworks with Intrinsic Peroxidase-Like Catalytic Activity as a Colorimetric Biosensing Platform. *Chem. Commun.* **2014**, *50*, 1092−1094.
(20) Vázquez-González, M.; Liao, W.-C.; Cazelles, R.; Wang, S.; Yu, X.; Gutkin, V.; Willner, I. Mimicking Horseradish Peroxidase Functions Using Cu^{2+}-Modified Carbon Nitride Nanoparticles or Cu^{2+}-Modified Carbon Dots as Heterogeneous Catalysts. *ACS Nano* **2017**, *11*, 3247−3253.
(21) Song, Y.; Qu, K.; Zhao, C.; Ren, J.; Qu, X. Graphene Oxide: Intrinsic Peroxidase Catalytic Activity and Its Application to Glucose Detection. *Adv. Mater.* **2010**, *22*, 2206−2210.
(22) Wang, Y.-M.; Liu, J.-W.; Adkins, G. B.; Shen, W.; Trinh, M. P.; Duan, L.-Y.; Jiang, J.-H.; Zhong, W. Enhancement of the Intrinsic Peroxidase-Like Activity of Graphitic Carbon Nitride Nanosheets by ssDNAs and Its Application for Detection of Exosomes. *Anal. Chem.* **2017**, *89*, 12327−12333.
(23) Lin, T.; Zhong, L.; Jing, W.; Guo, L.; Wu, H.; Guo, Q.; Fu, F.; Chen, G. Graphite-Like Carbon Nitrides as Peroxidase Mimetics and Their Applications to Glucose Detection. *Biosens. Bioelectron.* **2014**, *59*, 89−93.
(24) Wang, N.; Han, Z.; Fan, H.; Ai, S. Copper Nanoparticles Modified Graphitic Carbon Nitride Nanosheets as a Peroxidase Mimetic for Glucose Detection. *RSC Adv.* **2015**, *5*, 91302−91307.
(25) Darabdhara, G.; Bordoloi, J.; Manna, P.; Das, M. R. Biocompatible Bimetallic Au-Ni Doped Graphitic Carbon Nitride Sheets: A Novel Peroxidase-Mimicking Artificial Enzyme for Rapid and Highly Sensitive Colorimetric Detection of Glucose. *Sens. Actuators, B* **2019**, *285*, 277−290.
(26) Peng, Y.; Lu, B.; Chen, L.; Wang, N.; Lu, J. E.; Ping, Y.; Chen, S. Hydrogen Evolution Reaction Catalyzed by Ruthenium Ion-Complexed Graphitic Carbon Nitride Nanosheets. *J. Mater. Chem. A* **2017**, *5*, 18261−18269.
(27) Tian, J.; Liu, Q.; Ge, C.; Xing, Z.; Asiri, A. M.; Al-Youbi, A. O.; Sun, X. Ultrathin graphitic carbon nitride nanosheets: a low-cost, green, and highly efficient electrocatalyst toward the reduction of hydrogen peroxide and its glucose biosensing application. *Nanoscale* **2013**, *5*, 8921−8924.
(28) Zhang, X.; Xie, X.; Wang, H.; Zhang, J.; Pan, B.; Xie, Y. Enhanced photoresponsive ultrathin graphitic-phase C_3N_4Nanosheets for bioimaging. *J. Am. Chem. Soc.* **2013**, *135*, 18−21.
(29) Agnès, C.; Arnault, J.-C.; Omnès, F.; Jousselme, B.; Billon, M.; Bidan, G.; Mailley, P. XPS Study of Ruthenium Tris-Bipyridine Electrografted from Diazonium Salt Derivative on Microcrystalline Boron Doped Diamond. *Phys. Chem. Chem. Phys.* **2009**, *11*, 11647−11654.
(30) Ye, H.; Mohar, J.; Wang, Q.; Catalano, M.; Kim, M. J.; Xia, X. Peroxidase-Like Properties of Ruthenium Nanoframes. *Sci. Bull.* **2016**, *61*, 1739−1745.
(31) Wei, J.; Chen, X.; Shi, S.; Mo, S.; Zheng, N. An Investigation of the Mimetic Enzyme Activity of Two-Dimensional Pd-Based Nanostructures. *Nanoscale* **2015**, *7*, 19018−19026.

DOI: 10.1021/acsami.9b10715
ACS Appl. Mater. Interfaces 2019, 11, 29072−29077